First Results from the Taiwan Axion Search Experiment with Haloscope in the 19.47–19.84 μeV Mass Range*

Ann Author[†] and Second Author[‡]
Authors' institution and/or address
*This line break forced with *

(TASEH Collaboration)

(Dated: March 17, 2022)

This Letter reports on the first results from the Taiwan Axion Search Experiment with Haloscope, a search for axions using a microwave cavity at frequencies between 4.707504 and 4.798147 GHz. Apart from the external signals, no candidates with a significance more than 3.355 were found. The experiment excludes models with the axion-two-photon coupling $|g_{a\gamma\gamma}| \gtrsim 7.8 \times 10^{-14}\,\mathrm{GeV}^{-1}$, a factor of ten above the benchmark KSVZ model for the mass range $19.47 < m_a < 19.84\,\mu$eV, reaching a sensitivity three orders of magnitude better than any existing limits. It is also the first time that a haloscope-type experiment places constraints on the $|g_{a\gamma\gamma}|$ in this mass region.

The axion is a hypothetical particle predicted as a consequence of a solution to the strong CP problem [1–3]. The solution proposed by Peccei and Quinn is to introduce a new global Peccei-Quinn $\mathrm{U(1)_{PQ}}$ symmetry that is spontaneously broken; the axion is the pseudo Nambu-Goldstone boson of $\mathrm{U(1)_{PQ}}$ [1]. Axions are abundantly produced during the QCD phase transition in the early universe and may constitute the dark matter (DM). Axions could be detected and studied via their two-photon interaction, the so-called "inverse Primakoff effect". The detectors with the best sensitivities to axions with a mass of $m_a \approx \mu$eV, as first put forward by Sikivie [4, 5], are haloscopes consisting of a microwave cavity immersed in a strong static magnetic field and operated at a cryogenic temperature. In the presence of an external magnetic field, the ambient oscillating axion field drives the cavity and they resonate when the frequencies of the electromagnetic modes in the cavity match the microwave frequency f, where f is set by the total energy of the axion: $hf = E_a = m_a c^2 + \frac{1}{2} m_a v^2$. The axion signal power is further delivered to the readout probe followed by a low-noise linear amplifier. The axion mass is unknown, therefore, the cavity resonator must allow the possibility to be tuned through a range of possible axion masses.

The Axion Dark Matter eXperiment (ADMX) excluded the KSVZ benchmark model within the mass range of 1.9–4.2 μeV and the DFSZ benchmark model for the mass ranges of 2.66–3.31 and 3.9–4.1 μeV, respectively [6–12]. The Haloscope at Yale Sensitive to Axion Cold dark matter (HAYSTAC) had performed searches first for the mass range of 23.15–24 μeV and later at around 17 μeV; they excluded axions with $|g_\gamma| \geq 1.38 |g_\gamma|^{\mathrm{KSVZ}}$ for $m_a = 16.96 - 17.12$ and 17.14–17.28 μeV [13]. The Center for Axion and Precision Physics Research (CAPP) constructed and ran simultaneously several experiments targeting at different frequencies; they have pushed the limits towards the KSVZ value within a narrow mass region of 10.7126–10.7186 μeV [14]. The QUest for AXions-$a\gamma$ (QUAX-$a\gamma$)

also pushed their limits close to the upper bound of the QCD axion-two-photon couplings for $m_a \approx 43\,\mu$eV [15]. This Letter presents the first results of a search for axions for the mass range of 19.47–19.84 μeV, from the Taiwan Axion Search Experiment with Haloscope (TASEH).

The signal power extracted from a microwave cavity on resonance is given by:

$$P_s = \left(g_\gamma^2 \frac{\alpha^2 \hbar^3 c^3 \rho_a}{\pi^2 \Lambda^4} \right) \times \left(\omega_c \frac{1}{\mu_0} B_0^2 V C Q_L \frac{\beta}{1+\beta} \right). \quad (1)$$

The first set of parentheses contains physical constants, a dimensionless model-dependent parameter g_γ, and the local dark-matter density $\rho_a = 0.45$ GeV/cm^3. The numerical values of g_γ are -0.97 and 0.36 in the Kim-Shifman-Vainshtein-Zakharov (KSVZ) [16, 17] and the Dine-Fischler-Srednicki-Zhitnitsky (DFSZ) [18, 19] benchmark models, respectively. For the QCD axions, the coupling constant $g_{a\gamma\gamma}$ that describes the strength of the axion-two-photon interaction in the Lagrangian is related to g_γ and the axion mass m_a:

$$g_{a\gamma\gamma} = \left(\frac{g_\gamma \alpha}{\pi \Lambda^2} \right) m_a, \quad (2)$$

where α is the fine-structure constant and $\Lambda = 78$ MeV is a scale parameter that can be derived from the mass and the decay constant of the pion and the ratio of the up to down quark masses. The second set of parentheses contains parameters related to the experimental setup: the angular resonant frequency of the cavity ω_c, the vacuum permeability μ_0, the nominal strength of the external magnetic field B_0, the volume of the cavity V, and the loaded quality factor of the cavity $Q_L = Q_0/(1+\beta)$, where Q_0 is the unloaded, intrinsic quality factor of the cavity and β is the coupling coefficient which determines the amount of coupling of the signal to the receiver. The form factor C is the normalized overlap of the electric field $\vec{E}$, for a particular cavity resonant mode, with the

external magnetic field $\vec{B}$:

$$C = \frac{\left[\int \left(\vec{B} \cdot \vec{E}\right) d^3\boldsymbol{x}\right]^2}{B_0^2 V \int E^2 d^3\boldsymbol{x}}. \tag{3}$$

Here, the magnetic field $\vec{B}$ points mostly along the axial direction of the cavity. The field strength has a small variation along the radial and axial directions and $B_0 \approx 7.8$ Tesla is the nominal magnetic field strength. For cylindrical cavities, the largest form factor is from the TM_{010} mode. The expected signal power derived from the experimental parameters of TASEH is $P_s \simeq 1.5 \times 10^{-24}$ W for a KSVZ axion with a mass of $19.5\,\mu$eV.

In the axion experiments, the figure of merit that determines the design of the experimental setup is the signal-to-noise ratio (SNR), i.e. the ratio of the signal power P_s to the fluctuation in the averaged noise power spectrum σ_n. According to Dicke's Radiometer Equation [20], the σ_n is given by:

$$\sigma_n = k_B T_{\rm sys}\sqrt{\frac{\Delta f}{t}} \tag{4}$$

where $T_{\rm sys}$ is the system noise temperature, an effective temperature associated with the total noise of the system, t is the data integration time t and Δf is the bandwidth over which a single measurement is made. The SNR will therefore be:

$$\begin{aligned} {\rm SNR} &= \frac{P_s}{\sigma_n}, \\ &= \frac{P_s}{k_B T_{\rm sys}}\sqrt{\frac{t}{\Delta f}}, \end{aligned} \tag{5}$$

One could see that the SNR is maximized by an experimental setup with a strong magnetic field, a large cavity volume, an efficient cavity resonant mode, a receiver with low system noise temperature, and a long integration time.

The system noise temperature $T_{\rm sys}$ has three major components:

$$T_{\rm sys} = T_{\rm b} + T_{\rm qn} + T_{\rm a}. \tag{6}$$

The three terms in Eq. (6) correspond to the effective temperatures of the following noise sources: (i) $T_{\rm b}$, the blackbody radiation from the cavity at a physical temperature $T_{\rm c}$, (ii) $T_{\rm qn} = \frac{1}{2}\,hf/k_B$, the quantum noise associated with the zero-point fluctuation of the vacuum, and (iii) $T_{\rm a}$, the noise added by the receiver (mainly from the first-stage amplifier). Apart from the flat baseline as described by Eq. (6), the noise spectrum observed by TASEH has an additional component with a Lorentzian shape due to the higher temperature at the cavity with respect to that in the dilution refrigerator. More details may be found in the Appendix of Ref. [21]. The Lorentzian component will be removed from the measured spectrum and only the baseline $T_{\rm sys}$ will be used

in the final analysis. Using the operation parameters of TASEH and the results from the calibration of readout electronics, the baseline value of $T_{\rm sys}$ for TASEH is about 2.1–2.4 K.

The detector of TASEH is located at the Department of Physics, National Central University, Taiwan and housed within a cryogen-free dilution refrigerator (DR) from BlueFors. A superconducting solenoid with a bore diameter of 76 mm and a length of 240 mm is integrated with the DR. The data for the analysis presented here were collected by TASEH from October 13, 2021 to November 15, 2021, and termed as the CD102 data, where CD stands for "cool down". During the data taking, the cavity sat in the center of the magnet bore and was connected via holders to the mixing flange of the DR at a temperature of $T_{\rm mx} \simeq 27$ mK. The temperature of the cavity stayed at $T_{\rm c} \simeq 155$ mK, higher with respect to the DR; it is believed that the cavity had an accidental thermal contact with the radiation shield in the DR. The cavity, made of oxygen-free high-conductivity (OFHC) copper, has an effective volume of $V = 0.234$ L and is a two-cell cylinder split along the axial direction. The cylindrical cavity has an inner radius of 2.5 cm and a height of 12 cm. In order to maintain a smooth surface, the cavity underwent the processes of annealing, polishing, and chemical cleaning. The resonant frequency of the TM_{010} mode can be tuned over the range of 4.667–4.959 GHz via the rotation of an off-axis OFHC copper tuning rod, from the position closer to the cavity wall to the position closer to the cavity center.

The CD102 data cover the frequency range of 4.707504–4.798147 GHz. In this Letter, all the frequencies in unit of GHz are quoted with six decimal places as the relative accuracy of frequency is 1 kHz. It shall be noted that the absolute accuracy of frequency is ≈ 10 kHz. There were 837 resonant-frequency steps in total, with a frequency difference of $\Delta f_{\rm s} = 95 - 115$ kHz between the steps. The value of $\Delta f_{\rm s}$ was kept within 10% of 105 kHz rather than a fixed value, such that the rotation angle of the tuning rod did not need to be fine-tuned and the operation time could be minimized; a 10% variation of the $\Delta f_{\rm s}$ is found to have no impact on the $|g_{a\gamma\gamma}|$ limits. Each resonant-frequency step is denoted as a "scan" and the data integration time was about 32-42 minutes. The integration time was determined based on the target $|g_{a\gamma\gamma}|$ limits and the experimental parameters; the variation of the integration time aimed to remove the frequency-dependence in the $|g_{a\gamma\gamma}|$ limits caused by frequency dependence of the added noise $T_{\rm a}$. The form factor C for the TM_{010} mode varies from 0.64 to 0.69 over the full frequency range. The intrinsic, unloaded quality factor Q_0 at the cryogenic temperature ($T_{\rm c} \simeq 155$ mK) is $\simeq 60000$ at the frequency of 4.74 GHz.

An output probe, made of a 50-Ω semi-rigid coaxial cable that was soldered to an SMA (SubMiniature version A) connector, was inserted into the cavity and its

depth was set for $\beta \simeq 2$. The signal from the output probe was directed to an impedance-matched amplification chain. The first-stage amplifier was a low noise high-electron-mobility transistor (HEMT) amplifier mounted on the 4K flange. The signal was further amplified at room temperature via a three-stage post-amplifier, and down-converted and demodulated to in-phase (I) and quadrature (Q) components and digitized by an analog-to-digital converter with a sampling rate of 2 MHz.

In order to perform a calibration for the amplification chain, the HEMT was connected to a heat source (a 50-Ω resistor) instead of the cavity; various values of input currents were sent to the source to change its temperature monitored by a thermometer. The power from the source was delivered following the same transmission line as that in the axion data running. The output power is fitted to a first-order polynomial, as a function of the source temperature, to extract the gain and added noise T_a for the amplification chain. The value of T_a is about $1.9-2.2$ K. A more detailed description of the TASEH detector, the operation of the data run, and the calibration of the gain and added noise temperature of the whole amplification chain can be found in Ref. [22].

The analysis of the TASEH CD102 data follows the procedure similar to that developed by the HAYSTAC experiment [23] and the details are described in Ref. [21]. The fast Fourier transform (FFT) algorithm is performed on the IQ time series data to obtain the frequency-domain power spectrum. The Savitzky-Golay (SG) filter [24] is applied to remove the structure of the background in the frequency-domain power spectrum. All the spectra from different frequency scans are combined with a weighting algorithm. In order to maximize the SNR, a running window of five consecutive bins in the combined spectrum is applied and the five bins within each window are merged to construct a final spectrum. The five frequency bins correspond to the 5-kHz axion signal line width, derived from the standard assumption of axion signal line shape as described by Eq. (7). This signal line shape is also used when defining the maximum likelihood weights for merging:

$$\mathcal{F}(f, f_a) = \frac{2}{\sqrt{\pi}} \sqrt{f - f_a} \left(\frac{3}{\alpha}\right)^{3/2} e^{\frac{-3(f - f_a)}{\alpha}}, \quad (7)$$

where $\alpha \equiv f_a \langle v^2 \rangle / c^2$. Here, the frequency f must be greater or equal to the axion frequency $f_a = m_a c^2 / h$. In this standard assumption of axion signal line shape, the DM halo density distribution is assumed to be spherically symmetric and close to be isothermal, which results in a velocity distribution similar to the Maxwell-Boltzmann distribution. Therefore, the variance $\langle v^2 \rangle$ and the most probable velocity (speed) v_p are related to each other: $\langle v^2 \rangle = 3v_p^2/2 = (270 \text{ km/s})^2$, where $v_p = 220$ km/s is the local circular velocity of DM in the galactic rest frame.

After the merging, if there were any potential signal with an SNR larger than 3.355, a rescan would be proceeded to check if it were a real signal or a statistical fluctuation. The procedure of the CD102 data taking was to perform a rescan after covering every 10 MHz; the rescan was done by adjusting the tuning rod of the cavity so to match the resonant frequency to the frequency of the candidate. In total, 22 candidates with an SNR greater than 3.355 were found. Among them, 17 candidates were from the fluctuations because they were gone after a few rescans. The remaining five candidates, in the frequency ranges of 4.710170 − 4.710190 GHz and 4.747301 − 4.747380 GHz, reached an SNR greater or equal to 5 after rescanning. The signals in the second frequency range were detected via a portable antenna outside the DR and found to come from the instruments in the laboratory, while the signals in the first frequency range were weaker but still present after turning off the external magnetic field. Therefore, these five candidates are considered external signals and no limits are placed for the above two frequency ranges.

Since no candidates were found after the rescan, the upper limits at 95% confidence level (C.L.) on the $|g_\gamma|$ and the $|g_{a\gamma\gamma}|$ are derived by setting the maximum SNR equal to five. Figure 1 shows the limits on the axion-two-photon coupling $|g_{a\gamma\gamma}|$ and the ratio of the limits on the dimensionless parameter $|g_\gamma|$ with respect to the KSVZ benchmark value ($|g_{\mathrm{KSVZ}}| = 0.97$). The analysis that merges bins without assuming a signal line shape results in $\approx 5.5\%$ larger values on the $|g_{a\gamma\gamma}|$ limits. If a Gaussian signal line shape with an FWHM of 2.5 kHz, about half of the axion line width in Eq. (7), is assumed instead, the limits will be $\approx 3.8\%$ smaller than the central results. Overall the total relative systematic uncertainty is $\approx 4.6\%$, coming from the uncertainties on the loaded quality factor Q_L, the coupling coefficient β, the added noise temperature T_a, the effect of the misalignment between the true axion frequency and the lower boundaries of the frequency bins, and the variation of the SG-filter parameters. The limits on $|g_{a\gamma\gamma}|$ range from $5.0 \times 10^{-14} \text{ GeV}^{-1}$ to $8.4 \times 10^{-14} \text{ GeV}^{-1}$, with an average value of $7.8 \times 10^{-14} \text{ GeV}^{-1}$; the lowest value comes from the frequency bins with additional eight times more data from the rescans, while the highest value comes from the frequency bins near the boundaries of the spectrum. Figure 2 displays the $|g_{a\gamma\gamma}|$ limits obtained by TASEH together with those from the previous searches. The results of TASEH exclude the models with the axion-two-photon coupling $|g_{a\gamma\gamma}| \gtrsim 7.8 \times 10^{-14} \text{ GeV}^{-1}$, a factor of ten above the benchmark KSVZ model for the mass range $19.47 < m_a < 19.84 \, \mu\text{eV}$ (corresponding to the frequency range of $4.707504 < f_a < 4.798147$ GHz).

After the collection of the CD102 data, the synthetic axion signals were injected into the cavity and read out via the same transmission line and amplification chain. The procedure to generate axion-like signals is summarized in Ref. [22] and the analysis of the synthetic axion
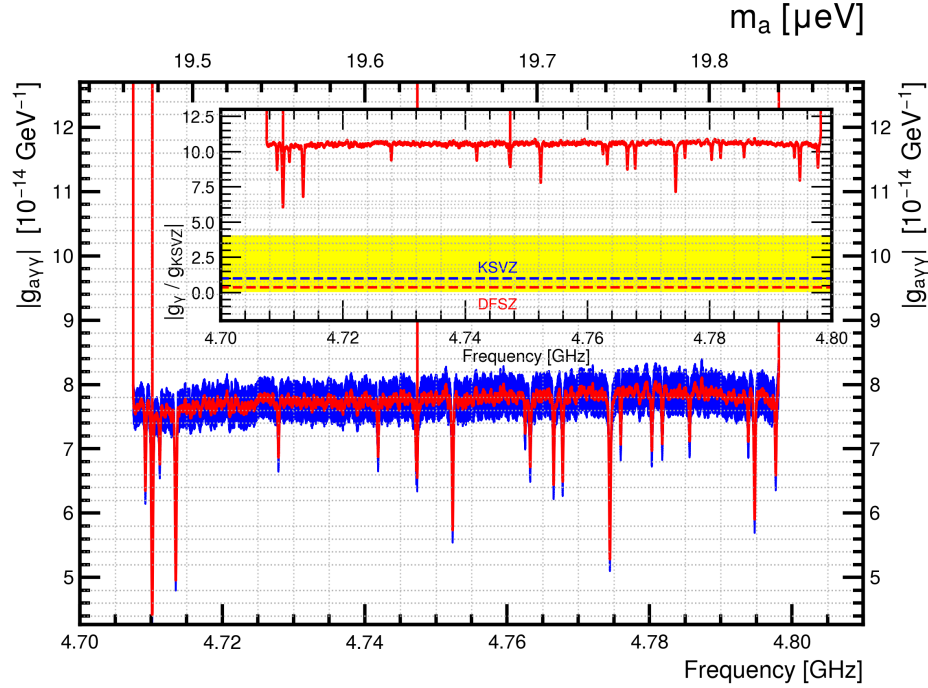
FIG. 1. The limits on $|g_{a\gamma\gamma}|$ and the ratio of the limits on $|g_\gamma|$ relative to $|g_{\mathrm{KSVZ}}| = 0.97$ (inset) for the frequency range of 4.707504–4.798147 GHz. The blue error band indicates the systematic uncertainties as discussed in Sec. **??**. The yellow band in the inset shows the allowed region of $|g_\gamma|$ vs. m_a from various QCD axion models, while the blue and red dashed lines are the values predicted by the KSVZ and DFSZ benchmark models, respectively

data is described in Ref. [21]. The analysis results of the synthetic axion signals prove that a power excess of more than 5σ can be found at the expected frequencies via the standard analysis procedure.

This Letter presents the first results of a search for axions for the mass range $19.47 < m_a < 19.84\,\mu\mathrm{eV}$. Apart from the external signals, no candidates with a significance more than 3.355 were found. The experiment excludes models with the axion-two-photon coupling $|g_{a\gamma\gamma}| \gtrsim 7.8 \times 10^{-14}\,\mathrm{GeV}^{-1}$ at 95% C.L., a factor of ten above the benchmark KSVZ model. The sensitivity on $|g_{a\gamma\gamma}|$ reached by TASEH is three orders of magnitude better than the existing limits. It is also the first time that a haloscope-type experiment places constraints in this mass region.

* A footnote to the article title
† Also at Physics Department, XYZ University.
‡ Second.Author@institution.edu

[1] R. D. Peccei and H. R. Quinn, CP conservation in the presence of pseudoparticles, Phys. Rev. Lett. **38**, 1440 (1977).

[2] S. Weinberg, A new light boson?, Phys. Rev. Lett. **40**, 223 (1978).

[3] F. Wilczek, Problem of strong p and t invariance in the presence of instantons, Phys. Rev. Lett. **40**, 279 (1978).

[4] P. Sikivie, Experimental tests of the "invisible" axion, Phys. Rev. Lett. **51**, 1415 (1983).

[5] P. Sikivie, Detection rates for "invisible"-axion searches, Phys. Rev. D **32**, 2988 (1985).

[6] C. Hagmann, D. Kinion, W. Stoeffl, K. van Bibber, E. Daw, H. Peng, L. J. Rosenberg, J. LaVeigne, P. Sikivie, N. S. Sullivan, D. B. Tanner, F. Nezrick, M. S. Turner, D. M. Moltz, J. Powell, and N. A. Golubev, Results from a high-sensitivity search for cosmic axions, Phys. Rev. Lett. **80**, 2043 (1998).

[7] S. J. Asztalos, E. Daw, H. Peng, L. J. Rosenberg, D. B. Yu, C. Hagmann, D. Kinion, W. Stoeffl, K. van Bibber, J. LaVeigne, P. Sikivie, N. S. Sullivan, D. B. Tanner, F. Nezrick, and D. M. Moltz, Experimental constraints on the axion dark matter halo density, The Astrophysical Journal **571**, L27 (2002).

[8] S. J. Asztalos, R. F. Bradley, L. Duffy, C. Hagmann, D. Kinion, D. M. Moltz, L. J. Rosenberg, P. Sikivie, W. Stoeffl, N. S. Sullivan, D. B. Tanner, K. van Bibber, and D. B. Yu, Improved rf cavity search for halo axions, Phys. Rev. D **69**, 011101 (2004).

[9] S. J. Asztalos, G. Carosi, C. Hagmann, D. Kinion, K. van Bibber, M. Hotz, L. J. Rosenberg, G. Rybka, J. Hoskins, J. Hwang, P. Sikivie, D. B. Tanner, R. Bradley, and J. Clarke, Squid-based microwave cavity search for dark-matter axions, Phys. Rev. Lett. **104**, 041301 (2010).

[10] N. Du, N. Force, R. Khatiwada, E. Lentz, R. Ottens, L. J. Rosenberg, G. Rybka, G. Carosi, N. Woollett, D. Bowring, A. S. Chou, A. Sonnenschein, W. Wester,
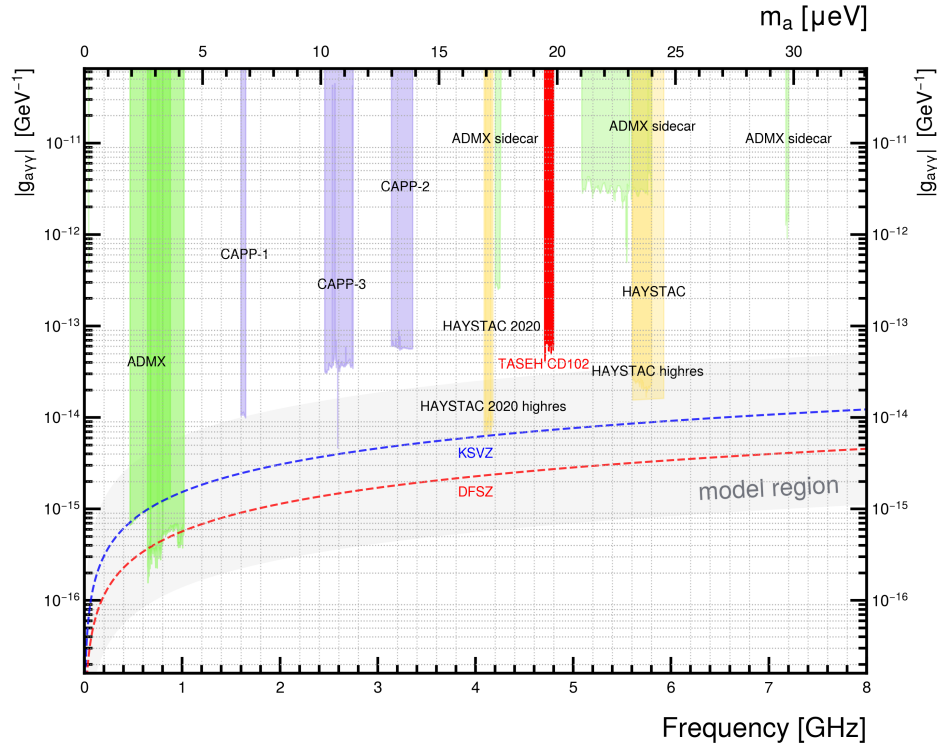
FIG. 2. The limits on the axion-two-photon coupling $|g_{a\gamma\gamma}|$ for the frequency ranges of 0–8 GHz, from the CD102 data of TASEH and previous searches performed by the ADMX, CAPP, and HAYSTAC Collaborations. The gray band indicates the allowed region of $|g_{a\gamma\gamma}|$ vs. m_a from various QCD axion models while the blue and red dashed lines are the values predicted by the KSVZ and DFSZ benchmark models, respectively.

C. Boutan, N. S. Oblath, R. Bradley, E. J. Daw, A. V. Dixit, J. Clarke, S. R. O'Kelley, N. Crisosto, J. R. Gleason, S. Jois, P. Sikivie, I. Stern, N. S. Sullivan, D. B. Tanner, and G. C. Hilton (ADMX Collaboration), Search for invisible axion dark matter with the axion dark matter experiment, Phys. Rev. Lett. **120**, 151301 (2018).

[11] T. Braine, R. Cervantes, N. Crisosto, N. Du, S. Kimes, L. J. Rosenberg, G. Rybka, J. Yang, D. Bowring, A. S. Chou, R. Khatiwada, A. Sonnenschein, W. Wester, G. Carosi, N. Woollett, L. D. Duffy, R. Bradley, C. Boutan, M. Jones, B. H. LaRoque, N. S. Oblath, M. S. Taubman, J. Clarke, A. Dove, A. Eddins, S. R. O'Kelley, S. Nawaz, I. Siddiqi, N. Stevenson, A. Agrawal, A. V. Dixit, J. R. Gleason, S. Jois, P. Sikivie, J. A. Solomon, N. S. Sullivan, D. B. Tanner, E. Lentz, E. J. Daw, J. H. Buckley, P. M. Harrington, E. A. Henriksen, and K. W. Murch (ADMX Collaboration), Extended search for the invisible axion with the axion dark matter experiment, Phys. Rev. Lett. **124**, 101303 (2020).

[12] C. Bartram *et al.* (ADMX Collaboration), Search for Invisible Axion Dark Matter in the 3.3–4.2 μeV Mass Range, Phys. Rev. Lett. **127**, 261803 (2021).

[13] K. M. Backes, D. A. Palken, S. A. Kenany, B. M. Brubaker, S. B. Cahn, A. Droster, G. C. Hilton, S. Ghosh, H. Jackson, S. K. Lamoreaux, and et al., A quantum enhanced search for dark matter axions, Nature **590**, 238–242 (2021).

[14] O. Kwon, D. Lee, W. Chung, D. Ahn, H. Byun, F. Caspers, H. Choi, J. Choi, Y. Chong, H. Jeong, J. Jeong, J. E. Kim, J. Kim, i. m. c. b. u. Kutlu, J. Lee, M. Lee, S. Lee, A. Matlashov, S. Oh, S. Park, S. Uchaikin, S. Youn, and Y. K. Semertzidis, First results from an axion haloscope at capp around 10.7 μeV, Phys. Rev. Lett. **126**, 191802 (2021).

[15] D. Alesini, C. Braggio, G. Carugno, N. Crescini, D. D'Agostino, D. Di Gioacchino, R. Di Vora, P. Falferi, U. Gambardella, C. Gatti, G. Iannone, C. Ligi, A. Lombardi, G. Maccarrone, A. Ortolan, R. Pengo, A. Rettaroli, G. Ruoso, L. Taffarello, and S. Tocci, Search for invisible axion dark matter of mass $m_a = 43$ μeV with the quax–$a\gamma$ experiment, Phys. Rev. D **103**, 102004 (2021).

[16] J. E. Kim, Weak Interaction Singlet and Strong CP Invariance, Phys. Rev. Lett. **43**, 103 (1979).

[17] M. A. Shifman, A. I. Vainshtein, and V. I. Zakharov, Can Confinement Ensure Natural CP Invariance of Strong Interactions?, Nucl. Phys. B **166**, 493 (1980).

[18] M. Dine, W. Fischler, and M. Srednicki, A Simple Solution to the Strong CP Problem with a Harmless Axion, Phys. Lett. B **104**, 199 (1981).

[19] A. R. Zhitnitsky, On Possible Suppression of the Axion Hadron Interactions. (In Russian), Sov. J. Nucl. Phys. **31**, 260 (1980).

[20] R. H. Dicke, The measurement of thermal radiation at microwave frequencies, Review of Scientific Instruments **17**, 268 (1946), https://doi.org/10.1063/1.1770483.

[21] Y.-H. Chang *et al.*, Taiwan Axion Search Experiment

with Haloscope: CD102 Analysis Details, (2022).

[22] Y.-H. Chang *et al.*, Taiwan Axion Search Experiment with Haloscope, (2022).

[23] B. Brubaker, L. Zhong, S. Lamoreaux, K. Lehnert, and K. van Bibber, Haystac axion search analysis procedure, Physical Review D **96**, 10.1103/physrevd.96.123008

(2017).

[24] A. Savitzky and M. J. E. Golay, Smoothing and differentiation of data by simplified least squares procedures, Anal. Chem. **36**, 1627 (1964).